Available online at www.sciencedirect.com
SCIENCE DIRECT®
Journal of Non-Crystalline Solids 319 (2003) 154–162
JOURNAL OF NON-CRYSTALLINE SOLIDS
www.elsevier.com/locate/jnoncrysol

Iron and iron oxide particle growth in porous Vycor glass; correlation with optical and magnetic properties

D. Sunil [a], H.D. Gafney [a,*], M.H. Rafailovich [b], J. Sokolov [b], R.J. Gambino [b], D.M. Huang [c]

[a] *Department of Chemistry and Biochemistry, City University of New York, Queens College, Flushing, NY 11367, USA*
[b] *Department of Material Science and Engineering, State University of New York, Stony Brook, NY 11794, USA*
[c] *AT&T Bell Laboratories, Crawfords Corners, Holmdel, NJ 07733, USA*

Received 26 November 2001; received in revised form 3 September 2002

Abstract

The growth of elemental iron and iron oxide particles derived from the photolysis of $Fe(CO)_5$ adsorbed onto porous Vycor glass has been characterized and correlated with the optical and magnetic properties of the particles. Photolysis does not result in particle growth per se. Photolysis causes extensive diffusion of the precursor, which leads to a high surface coverage in the outer volumes of the glass and the formation of small, $\leqslant 1$ nm in diameter particles consisting of an elemental iron core with an Fe_2O_3 coating. Particle growth occurs during the subsequent heating with the majority of growth occurring at temperatures of $\leqslant 700$ °C. The resultant particle size in the consolidated glass is equivalent to initial pore size in the glass, 10 ± 1 nm, and the inter-particle spacing equivalent to the correlation length of the porous glass, 24 ± 1 nm implying particle size and spacing are defined by the morphology of the porous glass. The 10 ± 1 nm diameter particles consist of an $\approx$8 nm diameter Fe^0 core surrounded by 1 nm thick α-Fe_2O_3 cladding. Particle growth is accompanied by a decline in optical transparency and a conversion from superparamagnetism to ferromagnetism with the particles exhibiting a large coercivity. The latter is attributed to an exchange anisotropy between the Fe^0 core and the oxide which becomes distributed throughout the body of the 10 ± 1 nm diameter particles.

1. Introduction

Photopatterning metals and/or metal oxides in porous, glassy matrices and thermally consolidating the matrix to a non-porous glass creates refractive index gradients in the glass [1–10]. A 488 nm photolysis of $Fe(CO)_5$ physisorbed onto porous Vycor glass (PVG), or porous substrates derived from the base-catalyzed polymerization of tetramethoxysiliane, ethanol and water (TMOS/EtOH/H_2O), for example, increases the refractive index of the exposed region relative to the bulk glass. Heating removes the unreacted precursor, $Fe(CO)_5$, and consolidates the matrix without loss of pattern resolution thereby creating refractive index gradients that, depending on their shape, guide, focus, or diffract light [11–13]. Consolidation of the matrix eliminates scattering arising

* Corresponding author. Tel.: +1-718 997 4114; fax: +1-718 997 5531.
E-mail address: hgafney@qc1.qc.edu (H.D. Gafney).

0022-3093/03/$ - see front matter © 2003 Elsevier Science B.V. All rights reserved.
doi:10.1016/S0022-3093(02)01913-0

from the porosity of the glass and achieves long-term thermal stability. However, it is often at the expense of optical performance. In systems created via photolysis of 10^{-4} mol of $Fe(CO)_5$ adsorbed on to PVG, which leads to the deposition of elemental iron, Fe^0, and α-Fe_2O_3, [14–16] for example, 50% T shifts from the 300–350 nm region immediately after photolysis to the 650–700 nm region after consolidation of the glass matrix [11–13].

In addition to optical performance, the physical properties of the deposits change during the thermal treatments. The photoproducts deposited in PVG exhibit superparamagnetism, [15] whereas consolidation of the matrix at 1200 °C converts the photoproduct to a ferromagnetic material with an exceptional large coercivity [15]. As yet, no set of experimental conditions, including changing the excitation wavelength or increasing the initial $Fe(CO)_5$ loading, leads directly to the photodeposition of a ferromagnetic material. Although the Fe^0 and α-Fe_2O_3 ratio varies somewhat from sample to sample, conversion to a ferromagnetic material occurs with little change in sample composition [14,15]. Since the magnetic properties of iron and iron oxide particles are functions of composition and size, [17–21] the appearance of ferromagnetism was tentatively attributed to the aggregation of the photoproducts [14,15].

These experiments were undertaken to identify factors that control particle growth in PVG during the photochemical deposition and the subsequent thermal consolidation steps, and to correlate particle size with the optical and magnetic properties of the deposits. Data presented here show that photolysis does not result in particle growth per se. Instead, photolysis changes the distribution of the precursor leading to a high surface coverage of small particles, $\leqslant 1$ nm in diameter, in the outer volumes of the glass. This creates a high surface coverage where subsequent particle growth is defined by the initial morphology of the porous glass. Particle growth occurs within the pores of the glass where agglomeration creates an ferromagnetic iron particle which, interlaced and surrounded by Fe_2O_3, is insensitive to oxidation and exhibits a high coercivity.

2. Experimental

2.1. Materials

$Fe(CO)_5$ was used without further purification since electronic and IR spectra of the vaporized compound agreed with published spectra [22]. Polished, 2.5 cm × 2.5 cm × 1.0 mm samples of code 7930 PVG were continuously extracted with distilled water for more than 24 h, dried at room temperature under vacuum, and calcined at 650 °C for at least 72 h [22]. The glass samples were stored at this temperature until needed, at which point the sample was removed and cooled to room temperature under vacuum.

Impregnation was accomplished by a previously described vapor deposition techniques [22]. The amount of $Fe(CO)_5$ adsorbed was determined by comparing the optical density of the impregnated samples to samples containing known amounts of $Fe(CO)_5$ [22]. The samples prepared in these experiments typically contain 10^{-4} mol of $Fe(CO)_5$/g of PVG. All samples were irradiated in air with 488 nm light from an Ar^+ laser.

2.2. Physical measurements

UV–visible spectra were recorded on a double-beam spectrophotometer relative to the unimpregnated glass. Thermal gravimetric and mechanical analyses and differential thermal analyses were performed on a commercial instrument calibrated with commercial standards. Surface areas of the porous glasses were determined by nitrogen adsorption. Mössbauer spectra were recorded on a spectrometer equipped with a 10 millicurie ^{57}Co/Rh source, and fit with Lorenzian functions using the least-squares test [15]. Transmission spectra were recorded either at room temperature or at 20 K using a low-temperature refrigerator. Magnetic properties of the samples were measured on a previously described vibrating sample magnetometer and a SQUID magnetometer [23]. Transmission electron micrographs were recorded at 400 keV, while X-ray microprobe analyses were carried out on the X26 beamline of the National Synchroton Light Source at Brookhaven National Laboratory.

3. Results

Photolysis dramatically changes the distribution of the $Fe(CO)_5$ precursor in the glass [15]. Initially uniformly distributed to at least a depth of $\geqslant 4000$ μm, as photolysis consumes the $Fe(CO)_5$ in the outer volumes of glass; however, unreacted $Fe(CO)_5$ diffuses from the interior to the outer volumes where it photochemically decomposes to Fe^0 and Fe_2O_3 [6,14,15]. Immediately after photolysis, the amount of iron in the outer 500–700 μm of the glass increases by a factor of approximately three relative to that initially present. The maximum in iron occurs at 100 μm, while that at depths greater than 800–900 μm declines to less 10% of that initially present [16]. In spite of the change in distribution, it is not accompanied by particle growth. Transmission electron microscopy (TEM) of the photolyzed sample fails to reveal particles $\geqslant 1$ nm in diameter indicating that the Fe^0 and Fe_2O_3 photoproducts exist either as individual molecular species, or small aggregates. The specific form of the photoproducts at this point is not known, but small aggregates, $\leqslant 1$ nm in diameter, and composed of an Fe^0 core surrounded by Fe_2O_3, appears to be the most likely form since Mössbauer spectra show that the Fe^0/Fe_2O_3 ratio is insensitive to oxidants such as air, or water evolved during the consolidation of the glass [14].

Particle growth occurs during the subsequent heating, and with the exception of a slight change in iron distribution due to the 30–40% reduction in sample size during consolidation, it occurs with no measurable change in iron distribution in the glass. 3–4 nm diameter particles are evident after heating the samples to 650 °C (Fig. 1). Heating to 1200 °C consolidates the glass and increases particle size further (Fig. 2). Some variation in particle size and spacing is evident in Fig. 2, as well as what appear to be aggregates of two or more particles. However, the variation is thought to arise from particles at different depths in the sample, while the clusters are attributed to superimposed images of individual particles at different depths in the sample since this is evident only in the thicker portions of the samples. In the ten samples examined in these experiments, containing $0.5 \pm 0.1\%$ Fe by weight, the particles are individual and spherical with a median diameter of 10 ± 1 nm (Fig. 3), and an average inter-particle spacing of 22 ± 1 nm.

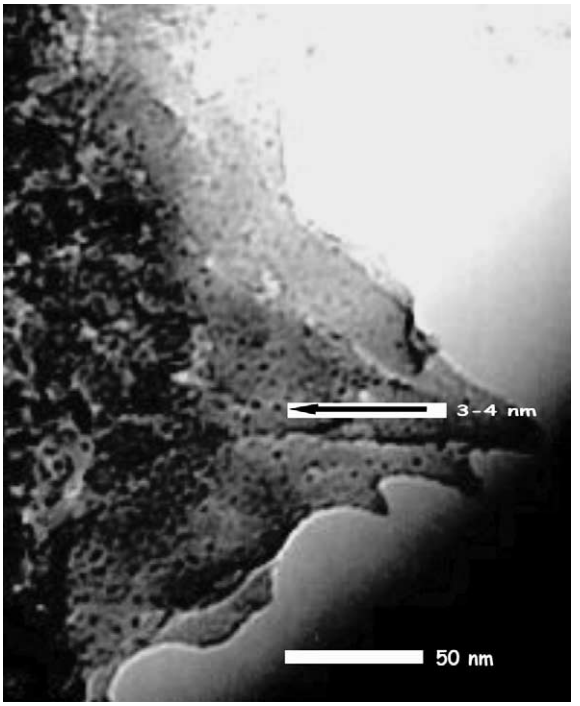

Fig. 1. TEM micrograph of photolyzed sample after heating to 650 °C.

Electronic spectra of the samples show that 50% T occurs in the 300–350 nm region immediately after photolysis, increases to the 450–500 nm region after heating to 650 °C and then to the 600–650 nm region after consolidating the glass at 1200 °C. Mössbauer spectra of the sample after photolysis, and after heating to 650 °C, consists of two doublets exhibiting isomer shifts of 0.52 ± 0.01 and 0.13 ± 0.01 mm/s, and quadrupole splittings of 0.64 ± 0.01 and 0.58 ± 0.01 mm/s [15]. No magnetic hyperfine structure is present in Mössbauer spectra, and the magnetization curves (Fig. 4(a)) do not exhibit hysterisis immediately after photolysis, or after heating the sample to 650 °C. Both the photoproduct and the 3–4 nm diameter particles (Fig. 1) exhibit superparamagnetism (Fig. 4(a)). Heating to 1200 °C consolidates the glass, and increases the particle size to 10 ± 1 nm in

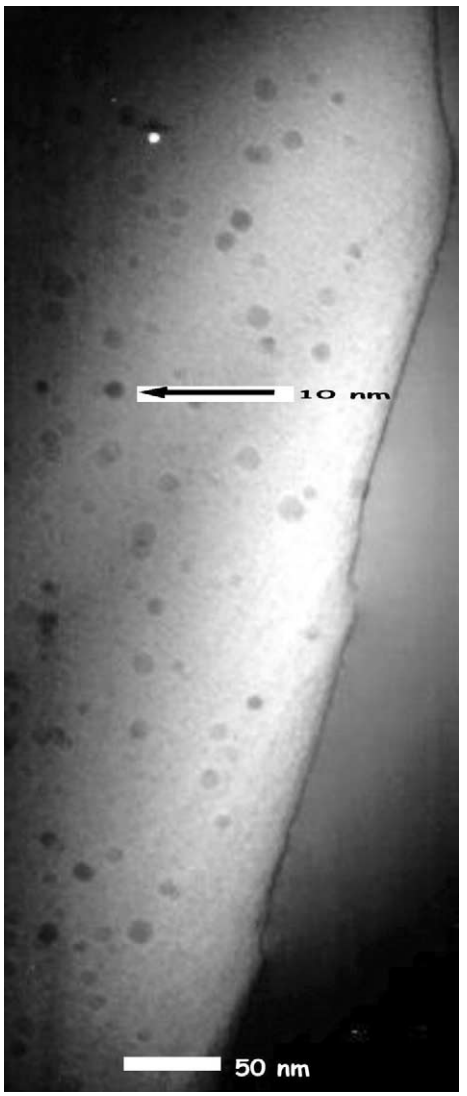

Fig. 2. TEM micrograph of photolyzed sample after consolidating the glass at 1200 °C.

diameter (Fig. 2). Mössbauer spectra of the consolidated samples exhibit two overlapping six line spectra with isomer shifts of 0.13 and 0.57 mm/s relative to metallic iron and magnetic hyperfine fields of 370 and 425 kG [15]. The 10 ± 1 nm diameter particles are ferromagnetic and exhibit a hysterisis corresponding to a coercivity of 965 kG (Fig. 4(b)).

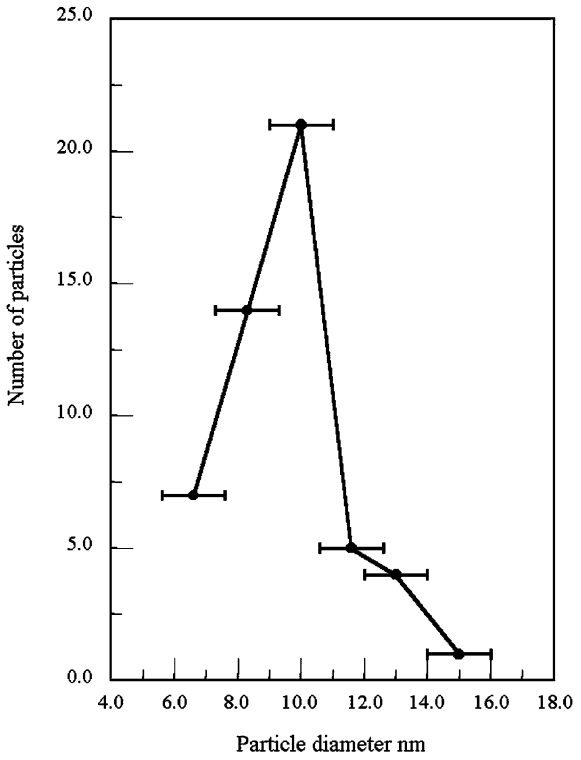

Fig. 3. Distribution of particle diameters in samples consolidated at 1200 °C.

4. Discussion

$Fe(CO)_5$ physisorbs onto PVG without disruption or significant distortion of its primary coordination sphere [22]. Photolysis of the adsorbed complex, designated $Fe(CO)_5$ (ads), with 488 nm light leads to decomposition with a quantum efficiency of 0.96 ± 0.05 [22]. No intermediates persisting for more than a few milliseconds are detected in the presence of air, and exposure to CO fails to regenerate $Fe(CO)_5$ (ads) indicating an irreversible oxidation of the adsorbed complex. Nevertheless, XANES and Mössbauer analyses of the photolyzed sample indicate the presence of elemental iron, Fe^0, and α-Fe_2O_3 in approximately equal amounts [14,15]. The Fe^0/Fe_2O_3 ratio varies somewhat from sample to sample with 53–65% of the deposited iron present as elemental iron after photolysis. The ratio declines slightly during the subsequent heating and consolidation of the glass,

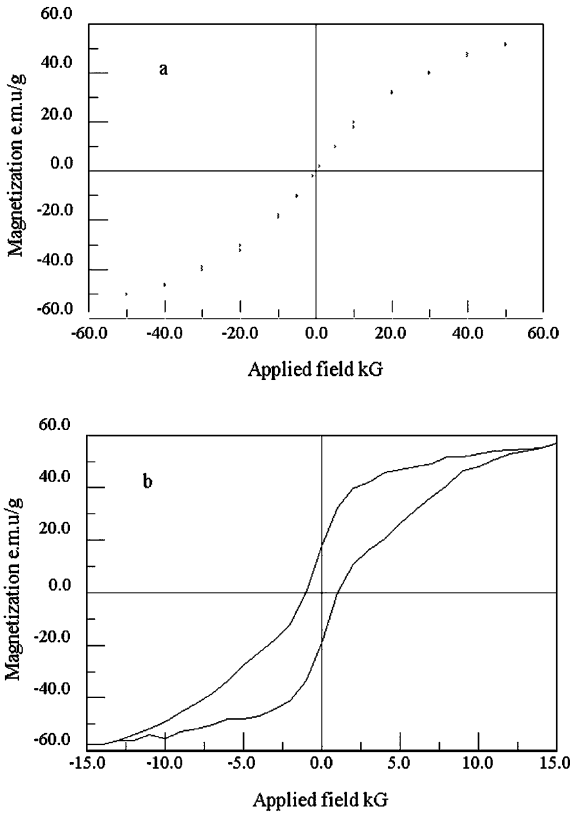

Fig. 4. Sample magnetization as a function of applied field for samples heated to (a) 650 and (b) 1200 °C.

but Mössbauer and XANES indicate that $42 \pm 12\%$ of the iron in the consolidated glass remains as elemental iron [14]. The absence of complete oxidation of the iron in the consolidated glass suggests that Fe^0 does not exist as an individual atoms since individual iron atoms would be spontaneously oxidized either by air during the subsequent heating, or water evolved during consolidation of the glass [24,25]. Five-nm diameter iron particles generated in air, for example, react immediately to form 1–2 nm thick oxide coatings, which subsequently curtailed the rate of further oxidation [26]. The lack of complete oxidation in PVG during the subsequent heating and consolidation suggests that the photoproducts are small aggregates, $\leqslant 1$ nm in diameter, containing an iron core surrounded by the oxide.

X-ray microprobe analyses reveal a uniform distribution of $Fe(CO)_5$ to a depth of $\geqslant 4000$ μm prior to photolysis [15,27]. Assuming a uniform distribution throughout the glass before photolysis [15,27], the surface area of PVG, 183 ± 15 m^2/g, and the projected area of $Fe(CO)_5$ on the surface, 0.3 $nm^2/Fe(CO)_5$ (ads), [22] indicate the loadings examined in these experiments, 10^{-4} mol of $Fe(CO)_5/g$, correspond to a fractional surface coverage of 0.10 ± 0.01. However, photolysis increases the amount of iron near the surface of the sample, i.e., within the first 100–200 μm, by a factor of approximately three, relative to that initially present, and reduces that at depths greater than 800–900 μm to less 10% of that present initially [16]. Time-resolved experiments establish that the change in iron distribution is due to diffusion of $Fe(CO)_5$ during photolysis [22]. As the photochemical reaction consumes $Fe(CO)_5$ in the outermost volumes of the glass, unreacted $Fe(CO)_5$ diffuses from the interior of the glass to these outer volumes where it undergoes photoinduced decomposition. The three fold increase in iron in the first 100–200 μm increases the loading to 3×10^{-4} mol of $Fe(CO)_5/g$ in the outer volume, which corresponds to fractional surface coverage of ≈ 0.30 or 1 $Fe(CO)_5$ molecule/nm^2. This increase in surface coverage allows the growth of $\leqslant 1$ nm diameter aggregates of Fe^0 and Fe_2O_3 to occur via diffusion of no more than a few nanometers.

Since $Fe(CO)_5$ desorbs from the glass at a relative low temperature, particle growth occurring during heating derives from the small aggregates created photochemically, as opposed to the thermal decomposition of the precursor. Furthermore, unlike the photochemical step, it occurs with no measurable change in iron distribution. Heating to 650 °C increases particle size to 3–4 nm in diameter (Fig. 2). If the particle consists of a central core of Fe^0 surrounded by Fe_2O_3, the equivalence of the relative intensities of the Mössbauer absorptions indicates equal numbers of iron atoms in the core and the cladding. Assuming their densities are equivalent to those of those of the bulk materials, 7.86 and 5.24 g/cm^3, respectively, setting the quotients of the mass of each present divided by their densities equal to the volume of the 4 nm particle indicates the 3–4 nm diameter particles consist of a

2 nm diameter Fe^0 core surrounded by 1 nm thick Fe_2O_3 layer. Although the data gathered in these experiments point to an oxide that most closely resembles α-Fe_2O_3, the result is consistent with previous studies which show that a 1 nm thick layer of Fe_3O_4 and/or γ-Fe_2O_3 shields the underlying elemental iron from further oxidation [26]. Formation of 3–4 nm diameter particles with no significant change in the Fe^0/Fe_2O_3 ratio implies aggregation occurs without compromising the integrity of the oxide coating. The specific structure of the particle is not known, but assuming spherical particles composed of an iron core surrounded by the oxide, particle growth at these lower temperatures appears to be a simple aggregation of the individual photoproducts.

Consolidating the glasses at 1200 °C increases the particle size to 10 ± 1 nm (Fig. 3), which is within experimental error of the diameter of the cavities present in the original sample of PVG, 10 ± 1 nm. Furthermore, the average inter-particle spacing, 22 ± 1 nm, is equivalent to the correlation length of the porous glass, 24 ± 2 nm [9,28]. The implication is the morphology of the porous glass controls the size of the particles and their spacing in the consolidated glass. This implies that the majority of particle growth must occur at temperatures below the softening point of the glass, which is about 700 °C [29]. Otherwise, loss of the original structure of the porous glass would be expected to produce a range of particle sizes and spacings. Particle growth within the cavities of the glass seems intuitive, but it is not mechanistically obvious how it occurs. Specifically, why does particle growth stop when the pores are filled and not continue within the interconnecting passages to produce a glass interlaced with Fe^0 and α-Fe_2O_3 rather than the spherical 10 ± 1 nm diameter particles evident in Fig. 2. The increased surface coverage created photochemically suggests that, at least in the outer volumes of the glass, particle growth may begin on all surfaces within the porous glass. However, the narrower passages collapse at faster rate than the larger pores, and the smaller particles within these narrow passages may be forced into the larger pores. When the pore is filled, consolidation forces the excess particles onto other cavities. This implies a range of smaller particles arising from the excess, but within the resolution of these experiments, there is no evidence of smaller particles, which leads us to suspect that particle growth is a chemical consequence of the composition of the pore and/or its surface, rather than a physical consequence of the structure of the glass. This is also supported by results obtained with other metal compounds. Similar changes in refractive index occur in glasses impregnated with $(CH_3)_3SnI$, for example [9,27]. However, X-ray microprobe analyses show no significant change in tin distribution after photolysis, and TEM analyses fail to reveal any particles $\geqslant 1$ nm in diameter after photolysis, or after heating and consolidation of the glass suggesting that particle size and distribution are not simply a function of the morphology of the support, but reflect instead the chemical nature of the surface and its interaction with the photoproduct.

The decline in optical transparency as well as the change from superparamagnetism to ferromagnetism arise from the increase in particle size since both occur with little change in sample composition. The isomer shifts and quadrupole splittings of the photoproducts and the 3–4 nm diameter particles, 0.52 ± 0.01 and 0.13 ± 0.01 mm/s, and 0.64 ± 0.01 and 0.58 ± 0.01 mm/s, respectively, correspond to the values reported for α-Fe_2O_3 and Fe^0 [15]. The photoproducts and the 3–4 nm diameter particles are superparamagnetic (Fig. 4(a)), but convert to a ferromagnetic material with a coercivity of 965 kG on consolidation as indicated by the appearance of overlapping six line spectra and magnetic hysterisis (Fig. 4(b)). Nevertheless, the isomer shifts, 0.13 and 0.57 mm/s, and magnetic hyperfine fields of 370 and 425 kG of the ferromagnetic material in the consolidated glass remain within the range of those reported for elemental iron and α-Fe_2O_3 [15,30–32]. Several investigators report six-line Mössbauer spectra for similar sized iron particles in metallic glasses, but the iron content in those glasses, 10–15% by weight, is considerably larger than the $<1\%$ used in these experiments [33–35]. The relative intensities of the Mössbauer absorptions and the XANES show no change in the Fe^0/α-Fe_2O_3 ratio indicating that the changes in the optical and magnetic

properties are due to the change in particle size rather than a compositional change.

The absence of ferromagnetism in the smaller 3–4 nm diameter particles is attributed to volume-dependent superparamagnetic relaxation. In small particles, the magnetic vector is not fixed along the easy direction as in macroscopic particles, but fluctuates. The relaxation time, τ, of a magnetized particle of volume V is given by Néel–Brown formula $\tau = \tau_0 \exp(KV/k_B T)$ where k_B is the Boltzmann constant, and K is the anisotropy energy constant [36,37]. Neel estimated τ_0, the relaxation time of an isolated, hypothetical, symmetrical particle to be on the order of 10^{-9} s, [38] although in recent years, τ_0 is customarily taken to be 10^{-10} s [17–19,38]. The absence of a magnetic hyperfine splitting in the Mössbauer spectrum of the 3–4 nm diameter particles at room temperature and at 20 K implies the Mössbauer Larmor precession time (10^{-8} s) [39] exceeds the magnetic relaxation time thereby reducing the average magnetization of the particle to zero. Consolidation at 1200 °C increases the particle diameter to 10 ± 1 nm. The increase in particle size increases the magnetic relaxation time to a point where it exceeds the Mössbauer Larmor precession time and measuring time of the magnetization. Consequently, the resulting particles exhibit a magnetic hyperfine splitting with magnetic hystersis and coercivity (Fig. 4). The appearance of a magnetic hyperfine structure in the room temperature Mössbauer spectrum of the consolidated samples implies the blocking temperature, T_b, exceeds room temperature. Taking T_b to be $\geqslant 22$ °C, a lower limit of the anisotropy energy constant is calculated to be 4.9×10^5 erg/cm^3. The value is larger than that reported for bulk iron, 10^5 erg/cm^3, and larger than that reported for Fe_2O_3, 10^4 erg/cm^3, but within the range reported for small particles [17,19,40–43].

High coercivity is not unusual for small iron particles [40–43]. In general, the coercivity of small particles increases as size decreases. For example, 16 nm diameter particles with a metallic core and oxide envelope exhibit a coercivity of 1580 Oe [42]. High coercivity arises from shape, surface and stress anisotropy, and inter-particle exchange interactions [44,45]. With an average spacing of 22 ± 1 nm between the particles, inter-particle exchange interactions are negligible and discounted. Coercivity arising from shape and stress anisotropy are also discounted since the particles are spherical (Figs. 1 and 2). Stress during particle growth is expected to produce non-spherical particles. Anisotropy values two orders of magnitude larger than that for bulk iron for 4.5 nm diameter Fe^0 particles deposited in SiO_2 led the suggestion that the iron is bound to the matrix [46]. EXAFS of the iron deposited in PVG, however, give no indication that Fe^0 in PVG is bound to the glass matrix [15]. On the other hand, several investigators attribute the high anisotropy and coercivity for small iron particles to an interaction between an iron core and surrounding oxide shell [47,48], while others attribute increases in coercivity from 100 to 900 Oe, as the particle diameter increases from 9 to 130 nm, to an exchange interaction between an iron core and a surrounding oxide layer [49]. Similarly, the high coercivity of cobalt particles is attributed to an exchange anisotropy between the ferromagnetic Co core and the anti-ferromagnetic CoO outer layer [50]. The insensitivity of the Fe^0/Fe_2O_3 ratio to air and the water evolved during consolidation points to elemental iron protected by an Fe_2O_3 coating. Consequently, the high coercivity of the particles formed in PVG is also attributed to an exchange anisotropy between an Fe^0 core and an Fe_2O_3 cladding about the core. Assuming a spherical particle (Fig. 2) consisting of an elemental iron core surrounded by the oxide, the diameter of the elemental iron core is calculated to be 6.8 nm with a 1.6 nm thick Fe_2O_3 coating. The core diameter is slightly smaller than the reported minimum diameter, 8.0 nm, necessary to achieve sufficient coercivity at 300 K to maintain magnetic alignment in Fe^0 particles deposited in an SiO_2 [48]. However, it is in excellent agreement with the diameter calculated from the linear relationship between iron core, d_c, and total particle diameter, d_t, i.e., $d_c = (0.85\, d_{total} - 1.5)$ nm [18]. The median particle diameter found in PVG, 10 ± 1 nm yields a diameter of the iron core of 7.0 ± 0.8 nm suggesting that the appearance of ferromagnetism in this Fe^0–Fe_2O_3–PVG system arises from the increase in particle size.

As noted above, the Fe^0–Fe_2O_3 particle growth occurs in the 10 ± 1 nm diameter pores of PVG,

but it is not simply a process of filling the pores with 3–4 nm particles (Fig. 1) to create a 10 ± 1 nm diameter particle (Fig. 2). Simple aggregation of smaller particles would be expected to retain the magnetic properties of the smaller particles, i.e., superparamagnetism. The appearance of ferromagnetism in the larger particles implies formation of a single particle. Furthermore, the 10 ± 1 nm diameter particles are spherical (Fig. 2) without any indication, at least at the level of resolution of this TEM data, $\leqslant 0.5$ nm, of structure that would be present as the result of simply filling the pores with a number of smaller particles. Instead, growth of the 10 ± 1 nm diameter particles must occur through a merging of the smaller particles into a single larger particle. Furthermore, since particle growth occurs with little change in the Fe^0/Fe_2O_3 ratio, particle growth must occur without loss of the integrity of the oxide coatings about the elemental iron cores. Consequently, agglomeration into a larger particle must involve either diffusion of the oxide layers of the smaller particles to the outside of the larger particles, or the larger ferromagnetic particles are not a spherical Fe^0 core surrounded by a uniformly thick Fe_2O_3 layer, but an Fe^0 core interlaced and coated with Fe_2O_3. Interlacing the oxide throughout an elemental iron core would dramatically increases the surface area of the oxide relative to that of elemental metal and reduce the separation between the two thereby increasing the coercivity of the particle. High coercivities have been found for small iron and iron oxide particles, although a dependence on the method of preparation, sample treatment and supporting matrix cloud the reason for the difficulty in magnetic reversibility. However, if the large coercivity of these particles reflects the distribution of Fe^0 and Fe_2O_3 throughout the particle, then the mechanism of particle growth could account for the observed dependence on preparation, treatment, and supporting matrix.

5. Conclusion

Photolysis of $Fe(CO)_5$ physisorbed onto PVG yields $\leqslant 1$ nm diameter Fe^0 and Fe_2O_3 particles. Annealing leads to particle growth with the final particle size, 10 ± 1 nm, and inter-particle spacing, 22 ± 1 nm, determined by the morphology of the porous glass. Particle growth shifts optical transparency further to the red, and changes the magnetic properties of the deposited particles from superparamagnetic to ferromagnetic with a high coercivity at room temperature. The high coercivity of the ferromagnetic particles, which are though to consist of an Fe^0 core, interlaced with and surrounded by Fe_2O_3, is attributed to exchange anisotropy between the elemental metal and the interdispersed oxide.

Acknowledgements

Support of this research by the National Science Foundation (DMR-9314033 and CHE-0079040), the Department of Defense/Air Force Office of Scientific Research (F49620-94-1-0209), the Petroleum Research Foundation and the New York State Science and Technology Foundation through the CUNY Ultrafast Photonics Materials and Applications Center for Advanced Technology is gratefully acknowledged. H.D.G. thanks Corning Inc. for samples of code 7930 PVG.

References

[1] N.F. Borrelli, D.L. Morse, J.W.H. Schreurs, J. Appl. Phys. 54 (1983) 3344.
[2] N.F. Borrelli, D.L. Morse, Appl. Phys. Lett. 43 (1983) 993.
[3] H.D. Gafney, J. Imag. Sci. 33 (1989) 37.
[4] H.D. Gafney, in: D. Perry (Ed.), Chemistry in Industry, American Chemical Society, Plenum, New York, NY, 1997, p. 189.
[5] H.D. Gafney, J. Macromol. Sci.-Chem. A 27 (9–11) (1991) 1187.
[6] E.A. Mendoza, D. Sunil, E. Wolkow, P. Wong, J. Sokolov, M.H. Rafailovich, M. den Boer, H.D. Gafney, Langmuir 7 (1991) 3046.
[7] E.A. Mendoza, E. Wolkow, M.H. Rafailovich, J. Sokolov, H.D. Gafney, A. Hansen, MRS Symp. Proc. 168 (1990) 381.
[8] D. Sunil, M.H. Rafailovich, J. Sokolov, H.D. Gafney, A. Hansen, MRS Symp. Proc. 168 (1990) 387.
[9] E.A. Mendoza, E. Wolkow, M.H. Rafailovich, J. Sokolov, H.D. Gafney, D. Sunil, G.G. Long, P.R. Jamian, Appl. Phys. Lett. 57 (1990) 209.

[10] E.A. Mendoza, PhD thesis, The City University of New York, 1992.
[11] D. Sunil, A.W. McQuade, H.D. Gafney, Appl. Spectrosc. 52 (1998) 1014.
[12] A.W. McQuade, D. Sunil, H.D. Gafney, Proc. of SPIE 139 (1998) 3778.
[13] A.W. McQuade, D. Sunil, H.D. Gafney, Appl. Spectrosc. 54 (6) (2000) 869.
[14] D. Sunil, M.H. Rafailovich, J. Sokolov, H.D. Gafney, Inorg. Chem. 32 (1993) 4489.
[15] H.D. Gafney, D. Sunil, M.H. Rafailovich, J. Sokolov, B. Kotyuhanski, B.J. Wilkins, A.L. Hanson, J. Appl. Phys. 74 (1993) 3768.
[16] D. Sunil, M.H. Rafailovich, J. Sokolov, H.D. Gafney, A. Hanson, B.J. Wilkens, M.L. den Boer, Mater. Res. Soc. Extented Abstr. 22 (1990) 191.
[17] F. Bodker, S. Morup, Europhys. Lett. 52 (2000) 217.
[18] S. Gangopadhyay, G.C. Hadjipanayis, B. Dale, C.M. Sorensen, K.J. Klabunde, V. Papaefthymiou, A. Kostikas, Phys. Rev. B 45 (1998) 3768.
[19] S.A. Majetich, Y. Jin, Science 284 (1999) 470.
[20] D. Zhang, K.J. Klabunde, C.M. Sorensen, G.C. Hadjipanayis, Phys. Rev. B 58 (1998) 14167.
[21] S. Wirth, V. Molnar, M. Field, D.D. Awschalom, J. Appl. Phys. 85 (1999) 5249.
[22] M.S. Darsillo, M. Paquette, H.D. Gafney, J. Am. Chem. Soc. 109 (1987) 3275.
[23] D. Sunil, M. Rafailovich, J. Sokolov, R.J. Gambino, C. Tsang, H.D. Gafney, D.M. Huang, J. Appl. Phys. 79 (8) (1996) 6025.
[24] A. Strawbridge, R.A. Rapp, G.I. Sproule, R.J. Hussey, M.J. Graham, J. Electrochem. Soc. 142 (7) (1995) 2301.
[25] A. Strawbridge, R.A. Rapp, J. Electrochem. Soc. 141 (7) (1994) 1905.
[26] S. Linderoth, S. Morup, M.D. Bentzon, J. Mater. Sci. 30 (1995) 3142.
[27] H.D. Gafney, J. Macromol. Sci.-Chem. A 27 (9–11) (1990) 1187.
[28] P. Wiltzius, F.S. Bates, S.B. Dierker, G.D. Wignall, Phys. Rev. A 36 (1987) 2991.
[29] J. Dong, PhD thesis, The City University of New York, 1997.
[30] J.R. Dormann, J.R. Cui, C. Sella, J. Appl. Phys. 57 (1985) 4283.
[31] G. Shirane, D.E. Cox, S.L. Ruby, Phys. Rev. 125 (1962) 1158.
[32] S. Morup, B. Topse, B.S. Clausen, Phys. Scripta 25 (1982) 713.
[33] I.S. Jacobs, C.P. Bean, in: G.T. Rado, H. Suhl (Eds.), Magnetism III, Academic Press, New York, 1963, p. 271.
[34] M.D. Dygar, Am. Mineral. 40 (1985) 304.
[35] J.R. Childress, C.L. Chien, M. Nathan, J. Appl. Phys. Lett. 56 (1990) 95.
[36] L. Neel, Ann. Geophys. 5 (1949) 99.
[37] W.F. Brown, J. Appl. Phys. 30 (1959) 130.
[38] C.L. Chien, G. Xiao, S.H. Liou, J.N. Taylor, A. Levy, J. Appl. Phys. 61 (1987) 3311.
[39] (a) P.E. Dickson, F.J. Berry, Mössbauer Spectroscopy, Cambridge University, Cambridge, UK, 1986, p. 5;
(b) P. Debrunner, H. Frauenfelder, in: L. May (Ed.), Introduction to Mössbauer Spectroscopy, Plenum, New York, NY, 1971 (Chapter 1).
[40] T. Shinjo, J. Phys. Colloq. 40 (1979) 63.
[41] C.F. Kerjnojan, K.J. Klabunde, C.M. Sorensen, G.C. Hadjipanayis, J. Appl. Phys. 67 (1990) 5897.
[42] Y. Wei, J. Wu, H. Lu, T. Xiangwang, Z. Qiu, H. Tang, J.C. Walker, J. Appl. Phys. 61 (1987) 3314.
[43] C.L. Chien, G. Xiao, S.H. Liou, S.J.N. Taylor, A. Levy, J. Appl. Phys. 61 (1987) 3311.
[44] G. Xiao, C.L. Chien, J. Appl. Phys. 63 (1988) 4252.
[45] A.H. Morrish, The Physical Principles of Magnetism, Robert E. Krieger, New York, 1980, p. 340.
[46] V. Papaefthymiou, A. Kostikas, A. Simopoullous, D. Niarchos, S. Gangopadyay, G.C. Hadjipanayis, C.M. Sorensen, K.J. Klabunde, J. Appl. Phys. 67 (1990) 4487.
[47] C.D. Graham, Phy. Rev. 112 (1958) 1117.
[48] J.L. Dorman, P. Gibart, G. Suran, C. Sella, Physica 86–88B (1977) 1431.
[49] W.H. Meiklejohn, C.P. Bean, Phy. Rev. 102 (1956) 1413.
[50] G.C. Hadjipanayis, Z. Tang, Z.S. Gangopadhyay, L. Yiping, C.M. Sorensen, K.J. Klabunde, A. Kostikas, V. Papaefthymion, in: J.L. Dormann, D. Fiorani (Eds.), Magnetic Properties of Fine Particles, North Holland, 1992, p. 35.